Journal of Statistical Physics, Vol. 98, Nos. 3/4, 2000

Lyapunov Instability for a Hard-Disk Fluid in Equilibrium and Nonequilibrium Thermostated by Deterministic Scattering

Christoph Wagner[1]

Received August 17, 1999; final September 30, 1999

We compute the full Lyapunov spectra for a hard-disk fluid under temperature gradient and under shear. The Lyapunov exponents are calculated using a recently developed formalism for systems with elastic hard collisions. The system is thermalized by deterministic and time-reversible scattering at the boundary, whereas the bulk dynamics remains Hamiltonian. This thermostating mechanism allows for energy fluctuations around a mean value which is reflected by only two vanishing Lyapunov exponents in equilibrium and nonequilibrium. In nonequilibrium steady states the phase-space volume is contracted on average, leading to a negative sum of the Lyapunov exponents. Since the system is driven inhomogeneously we do not expect the conjugate pairing rule to hold, which is indeed shown to be the case. Finally, the Kaplan–Yorke dimension and the Kolmogorov–Sinai entropy are calculated from the Lyapunov spectra.

KEY WORDS: Lyapunov exponents; equilibrium and nonequilibrium steady states; hard-disk fluid; computer simulations.

I. INTRODUCTION

Transport of energy and momentum is a central problem in nonequilibrium statistical mechanics, but so far most of our knowledge is confined to the macroscopic level. There is still a long way to go when it comes to understanding the phenomena in microscopic terms although significant progress has been made during the last years, with help from dynamical systems theory and computer simulations. External forces are needed to drive a system out of equilibrium, but in order to prepare a nonequilibrium steady state the redundant energy has to be removed thus preventing the

[1] Center for Nonlinear Phenomena and Complex Systems, Université Libre de Bruxelles, Campus Plaine Code Postal 231, Boulevard du Triomphe, B-1050 Brussels, Belgium.

0022-4715/00/0200-0723$18.00/0

system from heating up infinitely. One way out is the introduction of thermostating mechanisms[1–6] to the system. Both stochastic[7–14] and deterministic/time-reversible thermostats are in use, the latter having been introduced to ensure consistency with Hamiltonian dynamics.

Recently, an alternative thermostating mechanism has been proposed by Klages *et al.*[15, 16] in order to thermalize a Lorentz gas in an electric field. The Lorentz disk is modeled as having infinitely many internal degrees of freedom thus acting through time-reversible deterministic scattering with the Lorentz particle as reservoir. Later, this thermostating mechanism has been applied to many-particle systems in nonequilibrium steady states, i.e., a hard disk fluid under temperatures gradient and under shear.[17] Here, the boundary acts as a reservoir and it was shown that thermostating by deterministic scattering is related to stochastic boundaries; in some sense the random generator is only replaced by an invertible chaotic map. The calculated transport coefficients have been found to be in agreement with the theoretical values obtained from kinetic theory. Furthermore, the deterministic character of this thermostating mechanism allows for a calculation of the phase space contraction rate with the result that only for special cases of the scattering rules and in the thermodynamic limit the conjectured identity between exponential phase space contraction and entropy production rates holds. Thus, the fact that a thermalizing mechanism is deterministic and time reversible is neither necessary nor sufficient to guarantee such an equality. In the present paper we further investigate the dynamical properties of the deterministically thermostated hard disk fluid by computing the full Lyapunov spectra and related quantities like the Kaplan–Yorke dimension or the Kolmogorov–Sinai entropy. In Section II we briefly recapitulate the model and its thermostating mechanism and Section III serves to outline the method used for computing the Lyapunov exponents.[18, 19] The results are presented in Section IV and conclusions are drawn in Section V.

II. MODEL

A hard disk fluid possesses both the virtues of being rather tractable for computer simulations and of allowing a comparison of the results with hydrodynamics and kinetic theory. This is the reason why we chose such a fluid to verify if thermostating by deterministic scattering also works for many-particles systems. Therefore, we consider a two-dimensional system of hard disks confined in a square box of length L with periodic boundary conditions along the x-axis, i.e., the left and right sides at $x = \pm L/2$ are identified. The N disks interact among themselves via elastic hard collisions, thus the bulk dynamics is purely conservative. In the following and

in all the numerical computations we use reduced units by setting the particle mass m, the disk diameter σ and the Boltzmann constant k_B equal to one. Now, denote with p_x^i, p_y^i and with p_x^f, p_y^f the tangential and normal momentum of a disk before and after a collision with the wall. Then the scattering prescription is given as[17]

$$(p_x^f, p_y^f) = \begin{cases} \mathfrak{T}^{-1} \circ \mathscr{M} \circ \mathfrak{T}(p_x^i, p_y^i), & p_x^i \geqslant 0 \\ \Pi \circ \mathfrak{T}^{-1} \circ \mathscr{M}^{-1} \circ \mathfrak{T}(p_x^i, p_y^i), & p_x^i < 0 \end{cases} \tag{1}$$

where $\mathfrak{T}$: $[0, \infty) \times [0, \infty) \to [0, 1] \times [0, 1]$ is the invertible map

$$(\zeta, \xi) = \mathfrak{T}(p_x, p_y) = (\mathrm{erf}(|p_x|/\sqrt{2T}), \exp(-p_y^2/2T)) \tag{2}$$

and $\mathscr{M}$: $[0, 1] \times [0, 1] \to [0, 1] \times [0, 1]$ is a two-dimensional, invertible, phase-space conserving chaotic map to be specified later. $\Pi(p_x, p_y) = (p_x, -p_y)$ only serves to produce the right sign for the backward scattering. The parameter T plays the role of a temperature.[17] Note that the colliding disk retains its tangential direction and that the scattering is reversible by construction. In ref. 17, Eqs. (1) and (2) have been motivated via stochastic boundaries where the map $\mathscr{M}$ is essentially replaced by a two-dimensional random generator.

So far, the model has only been defined in equilibrium. In order to drive the model to a nonequilibrium steady state (NSS) the collision rule has to be modified appropriately. With T being the temperature of the fluid in equilibrium, a natural way of imposing a temperature gradient on the fluid is thus simply to choose different T's for the upper and the lower wall. The principle idea behind the shear modeling is to add somehow an additional shift along the direction of the moving wall during the collision. In the previous work[17] three different shear prescriptions have been proposed the first two being time-reversible and the third not. For brevity we consider here only the first and the third model. One way to model moving walls is to add some tangential momentum d to p_x before and after the collision of a particle with the boundary (model I in ref. 17),

$$(p_x^f, p_y^f) = \begin{cases} \mathscr{S}_d \circ \mathfrak{C}^+ \circ \mathscr{S}_d(p_x^i, p_y^i), & p_x^i \geqslant -d \\ \mathscr{S}_d \circ \mathfrak{C}^- \circ \mathscr{S}_d(p_x^i, p_y^i), & p_x^i < -d \end{cases} \tag{3}$$

with

$$\mathscr{S}_d(p_x^i, p_y^i) = (p_x^i + d, p_y^i) \tag{4}$$

and $\mathfrak{C}^+$, $\mathfrak{C}^-$ denoting the forward resp. backward scattering in Eq. (1). In order to impose a shear the shift d has only to be chosen with different signs for the upper and the lower wall. Note that these scattering rules are

time reversible. Another scattering rule (model III in ref. 17), which also models moving walls, reads:

$$(p'_x, p'_y) = \mathfrak{T}_*^{-1} \circ \mathscr{M} \circ \mathfrak{T}_*(p_x, p_y) \tag{5}$$

with

$$\mathfrak{T}_*(p_x, p_y) = \left(\frac{\mathrm{erf}[(p_x - d)/\sqrt{2T}] + 1}{2}, \exp(-p_y^2/2T) \right) \tag{6}$$

Model III is still deterministic but no longer time reversible and only using this shear model a (numerical) equality between phase space contraction rate and entropy production was found in ref. 17.

Having fixed our models we turn now to the calculation of the Lyapunov spectra.

III. METHOD

Like all hard disk systems our model is chaotic in the sense that two nearby phase space trajectories diverge exponentially with time. This is mainly due to the dispersing action of the hard disk collisions in the bulk, but especially for small particle numbers we also expect a contribution to this divergence due the chaotic nature of our scattering mechanism. The average logarithmic divergence rate in phase space are described by the so-called Lyapunov exponents λ_l. Denote by $\mathbf{\Gamma} = \{\mathbf{q}_1, \mathbf{q}_2, \mathbf{q}_N, \mathbf{p}_1, \mathbf{p}_2, ..., \mathbf{p}_N\}$ the 4N dimensional phase space vector for N disks. The time evolution

$$\mathbf{\Gamma}(t) = \Phi^t[\mathbf{\Gamma}(0)] \tag{7}$$

of an initial state $\mathbf{\Gamma}(0)$ consists of a smooth streaming which is interrupted by particle-particle and particle-wall collisions. Next, consider a satellite trajectory $\mathbf{\Gamma}_s(t)$ initially displaced from the reference trajectory by an infinitesimal vector $\delta\mathbf{\Gamma}(0)$. In a chaotic system $|\delta\mathbf{\Gamma}(0)|$ is growing on average exponentially, thus rendering the system unpredictable for long times. Then there exists a complete set of linearly independent initial vectors $\{\delta\mathbf{\Gamma}_l(0): l = 1, ..., 4N\}$ and Lyapunov exponents defined as[20]

$$\lambda_l = \lim_{t \to \infty} \frac{1}{t} \ln \frac{|\delta\mathbf{\Gamma}_l(t)|}{|\delta\mathbf{\Gamma}_l(0)|} \tag{8}$$

The λ_l, which we order according to $\lambda_1 \geqslant \lambda_2 \geqslant \cdots \geqslant \lambda_{4N}$, are independent of the coordinate system and the metric. The whole set of Lyapunov exponents is referred to as Lyapunov spectrum.

In Hamiltonian systems the Lyapunov exponents appear in pairs summing up to zero, $\lambda_i + \lambda_{4N-i+1} = 0$ for $i = 1,..., 2N$, due to the symplectic nature of the equations of motion. In a continuous dynamical system one Lyapunov exponent associated with the direction of the phase flow vanishes. Moreover, each conserved quantity leads to an additional vanishing Lyapunov exponent. The symmetry found in symplectic dynamical systems is lost when the system is driven to a nonequilibrium stationary state. However, for homogeneous driving the symmetry is replaced by the so-called *conjugate pairing rule*[21] asserting that after excluding the vanishing exponents associated with the flow direction and the conservation of energy the remaining pairs, i.e., $\{\lambda_1, \lambda_{4N}\}$, $\{\lambda_2, \lambda_{4N-1}\}$, and so on, each sum up to the same negative value C. For inhomogeneously driven systems such as ours or the Chernov–Lebowitz shear flow model,[12, 19] however, the symmetry is lost and no pairing rules exists.

As can be seen from Eqs. (1) and (2) the phase space volume is in general changed during each disk-wall collision. In equilibrium this averages up to zero, whereas in NSS the average phase space contraction rate is negative and is given by the sum of all Lyapunov exponents. Consequently, the phase volume shrinks continuously in NSS and the phase-space distribution collapses onto a multifractal strange attractor. The fractal dimension of this strange attractor can be estimated with the conjecture of Kaplan–Yorke,[22]

$$D_{\mathrm{KY}} = n + \frac{\sum_{l=1}^{n} \lambda_l}{|\lambda_{n+1}|} \tag{9}$$

where n is the largest integer for which $\sum_{l=1}^{n} \lambda_l \geqslant 0$. D_{KY} is the dimension of a phase space object which neither shrinks nor grows and for which the natural measure is conserved by the flow.

For the calculation of the full Lyapunov spectrum we use a method worked out by Dellago *et al.*[18, 19] which is actually a generalization of the algorithm of Benettin *et al.*[23] for smooth dynamical systems. The latter follows the time evolution of a reference trajectory and of a complement set of tangent vectors by solving the original and the linearized equations of motion, respectively. Periodic reorthonormalization prevents the tangent vectors from collapsing all into the direction of fastest growth. Averaging the logarithmic expansion and contraction rates of the tangent vectors then yields the Lyapunov exponents. For a hard disk system the free streaming is interrupted by impulsive collisions, either with another particle or the boundary. This certainly affects both the trajectory *and* the tangent space and has to be included in the calculation. The free streaming and the particle-particle collisions in the bulk have been treated in Section III-D of

ref. 18. We refer to Eqs. (39)–(42) and Eqs. (68)–(73) of this article for explicit expressions of the particle-particle collision rules in phase space and tangent space, respectively. It remains to consider the particle-wall collisions and the following lines are formulated in parallel to the respective treatment of Dellago and Posch for the Chernov–Lebowitz model.[19] In fact, the main difference lies in the "scattering matrix" and its derivatives.

If particle k collides with the walls its position remains unchanged whereas its momentum is changed according to the scattering rules Eq. (1). The collision map $\mathbf{\Gamma}^f = \mathbf{M}(\mathbf{\Gamma}^i)$ in phase space becomes, in the notation of ref. 18

$$\mathbf{q}_j^f = \mathbf{q}_j^i \qquad \text{for} \quad j = 1,..., N \tag{10}$$

$$\mathbf{p}_j^f = \mathbf{p}_j^i \qquad \text{for} \quad j \neq k \tag{11}$$

$$\mathbf{p}_k^f = \mathfrak{C}^+(\mathbf{p}_k^i), \qquad \text{for} \quad p_x^i \geqslant 0 \tag{12}$$

$$\mathbf{p}_k^f = \mathfrak{C}^-(\mathbf{p}_k^i), \qquad \text{for} \quad p_x^i < 0 \tag{13}$$

$$\tag{14}$$

using the abbreviations $\mathfrak{C}^+ = \mathfrak{T}^{-1} \circ \mathscr{M} \circ \mathfrak{T}$ for the forward scattering and $\mathfrak{C}^- = \Pi \circ \mathfrak{T}^{-1} \circ \mathscr{M}^{-1} \circ \mathfrak{T}$ for the backward scattering (Eq. (1)).

In order to obtain the corresponding transformation for the tangent space vector $\delta\mathbf{\Gamma}$ at a particle-wall collision we assume that the collision takes place at phase point $\mathbf{\Gamma}$ at time τ_c. Then the satellite trajectory, displaced by the infinitesimal vector $\delta\mathbf{\Gamma}$, collides at a different phase point $\mathbf{\Gamma} + \delta\mathbf{\Gamma}_c$ at a different time $\tau_c + \delta\tau_c$. A linear approximation in phase space *and* time yields[18]

$$\delta\mathbf{\Gamma}^f = \frac{\partial \mathbf{M}}{\partial \mathbf{\Gamma}} \cdot \delta\mathbf{\Gamma}^i + \left[\frac{\partial \mathbf{M}}{\partial \mathbf{\Gamma}} \cdot \mathbf{F}(\mathbf{\Gamma}^i) - \mathbf{F}(\mathbf{M}(\mathbf{\Gamma}^i)) \right] \delta\tau_c \tag{15}$$

where $\mathbf{F}$ is the right hand side of the equation of motion during the free streaming,[18] and $\partial\mathbf{M}/\partial\mathbf{\Gamma}$ is the matrix of the derivatives of the full collision map with respect to the phase-space coordinates. Obviously, the delay time δ_c is a function of the phase point $\mathbf{\Gamma}^i$ and of the tangent vector $\delta\mathbf{\Gamma}^i$. For a disk-wall collision of the kth particle the delay time $\delta\tau_c$ is given by

$$\delta\tau_c = -\frac{(\delta\mathbf{q}_k \cdot \mathbf{n})}{(\mathbf{p}_k/m \cdot \mathbf{n})} \tag{16}$$

Here, $\mathbf{n}$ is the normal vector of the wall pointing into the simulation box. Since the scattering rules Eq. (1) for the momentum components is

independent of the position of the particle, the matrix $\partial \mathbf{M}/\partial \mathbf{\Gamma}$ has the form

$$\frac{\partial \mathbf{M}}{\partial \mathbf{\Gamma}} = \begin{pmatrix} \mathbf{1} & \mathbf{0} \\ \mathbf{0} & \partial \mathfrak{C}^{\pm}(\mathbf{p}^i)/\partial(\mathbf{p}^i) \end{pmatrix} \tag{17}$$

where $\mathbf{1}$ and $\mathbf{0}$ are the $2N \times 2N$ unit and zero matrices, respectively. $\partial \mathfrak{C}^{\pm}(\mathbf{p}^i)/\partial(\mathbf{p}^i)$ is the matrix of the derivatives of the outgoing momenta with respect to the incoming momenta and only the components of the colliding particle k are different from zero. From Eq. (15) the following transformation rules for the tangent vectors can be deduced:

$$\delta \mathbf{q}_j^f = \delta \mathbf{q}_j^i \qquad \text{for} \quad j \neq k \tag{18}$$

$$\delta \mathbf{p}_j^f = \delta \mathbf{p}_j^i \qquad \text{for} \quad j \neq k \tag{19}$$

$$\delta \mathbf{q}_k^f = \delta \mathbf{q}_k^i - (\mathbf{p}_k^f - \mathbf{p}_k^i)\, \delta \tau_c \tag{20}$$

$$\delta \mathbf{p}_k^f = \frac{\partial \mathfrak{C}^{\pm}(\mathbf{p}_k^i)}{\partial(\mathbf{p}_k^i)} \cdot \delta \mathbf{p}_k^i \tag{21}$$

Omitting for notational convenience the index k indicating the colliding particle we obtain from Eq. (1) the following expressions for the 2×2 matrix $(\partial \mathfrak{C}^{\pm}(\mathbf{p}_k^i)/\partial(\mathbf{p}_k^i))_{\alpha\beta} = \partial p_\alpha^f / \partial p_\beta^i$, $\alpha, \beta \in \{x, y\}$

$$\frac{\partial p_x^f}{\partial p_x^i} = (\mathbf{D}\mathscr{M})_{11} \exp[((p_x^f)^2 - (p_x^i)^2)/(2T)],$$

$$\frac{\partial p_x^f}{\partial p_y^i} = -(\mathbf{D}\mathscr{M})_{12} \frac{\tau p_y^i}{\sqrt{2T}} \exp[((p_x^f)^2 - (p_y^i)^2)/(2T)],$$

$$\frac{\partial p_y^f}{\partial p_x^i} = -(\mathbf{D}\mathscr{M})_{21} \frac{\sqrt{2T}}{\pi p_y^f} \exp[((p_y^f)^2 - (p_x^i)^2)/(2T)],$$

$$\frac{\partial p_y^f}{\partial p_y^i} = (\mathbf{D}\mathscr{M})_{22} \frac{p_y^i}{p_y^f} \exp[((p_y^f)^2 - (p_y^i)^2)/(2T)], \qquad \text{for} \quad p_x^i \geqslant 0$$

Here, $\mathbf{D}\mathscr{M}$ denotes the matrix of the derivatives of the chaotic map $\mathscr{M}$. Equations (22) and (23) are stated for positive tangential velocities, for negative tangential velocities $\mathscr{M}$ has only to be replaced by $\mathscr{M}^{-1}$, see Eq. (1).

Combining the free streaming with the transformation for the disk-disk and the disk-wall collisions, one is now able to follow the exact time evolution of the trajectory and of the tangent-space vector.

IV. RESULTS

Using the algorithm outlined in the previous section we are now able to calculate the full Lyapunov spectrum for our hard disk model with deterministic scattering at the boundary. As already mentioned we use reduced units by setting the particle mass m, the disk diameter σ and the Boltzmann constant k_B equal to unity. We define the number density by $\bar{n} = N/L^2$. For simulation we use a collision-to-collision approach and neighbor lists.[7] For an initial configuration the centers of the disks are positioned on a triangular lattice and the momenta are chosen from a Gaussian with zero mean. The total momentum is then set to zero and the momenta are rescaled to obtain the total kinetic energy $E_{\text{kin}} = N(T_u + T_d)/2$, T_u and T_d being the imposed "parametrical" temperatures of the upper and the lower wall, respectively.

A. Equilibrium

We first set both wall temperatures T_u, T_d equal to one and compute the full Lyapunov spectra for a four-particle system at number density $\bar{n} = 0.2$ using three different chaotic maps:

$$\mathcal{M}_B(\zeta, \xi) = (k\zeta, \xi/k) \qquad \text{modulo 1,} \quad \text{(baker map)} \tag{24}$$

$$\mathcal{M}_C(\zeta, \xi) = ((k+1)\,\zeta + \xi, k\zeta + \xi) \qquad \text{modulo 1,} \quad \text{(cat map)} \tag{25}$$

and

$$\mathcal{M}_S: \begin{cases} \xi' = \xi - \dfrac{k}{2\pi} \sin(2\pi\zeta), \\ \zeta' = \zeta + \xi' \end{cases} \qquad \text{modulo 1,} \quad \text{(standard map)} \tag{26}$$

with $0 \leqslant \zeta,\ \xi \leqslant 1$. $k \in 2\mathbb{N}$ is a parameter controlling the chaoticity of the map, i.e., the magnitude of the Lyapunov exponents.

The resulting spectra are shown in Fig. 1 where we have also plotted the Lyapunov spectrum for elastic reflection as reference. To display the conjugate pairs, the Lyapunov exponents are ordered as $\{\lambda_{2N-i+1}, \lambda_{2N+i}\}$, with $i = 1,..., 2N$. Errors are estimated as in ref. 19 from the convergence of the exponents as a function of simulation time such that the time-dependent exponents did not deviate more than $\pm\Delta\lambda$ from their mean values during the second half of the simulation run. For high accuracy more than 10^7 disk-disk collisions and more than $5 \cdot 10^6$ disk-wall were simulated yielding errors less than ± 0.001 for the exponents and less than ± 0.002 for the pair sums. In the case of elastic reflection four Lyapunov exponents vanish. One

exponent vanishes due to the neutral expansion behavior in the direction of the flow, a second due to the conservation of kinetic energy. The third and the fourth exponent are zero due to the translational invariance of the system in the x-direction and the preservation of the x-component of the total momentum.[19] For a hard disk system thermostated by deterministic scattering only two Lyapunov exponents vanish. The kinetic energy is now allowed to fluctuate around a mean value, so only the neutral expansion and the translational invariance remain. As we expect the maximum Lyapunov exponent increases with increasing chaoticity of the map, i.e., when going from a baker map ($k=2$) to a cat map ($k=2$) to a standard map ($k=100$) (Results not plotted here show a similar behavior when k is increased for a given map.). The pairing rule for these models is satisfied with an error of ± 0.002 in the pair sums. At this point we add a remark which might seem at first purely technical. For all simulations we used a symmetrical configuration, i.e., Eq. (1) is used for the upper wall whereas $\mathscr{M}$ and $\mathscr{M}^{-1}$ are interchanged in Eq. (1) for the lower wall. Using the same scattering rules for both walls results in an asymmetry and eventually in an asymmetric Lyapunov spectrum even in equilibrium violating the pairing rule.

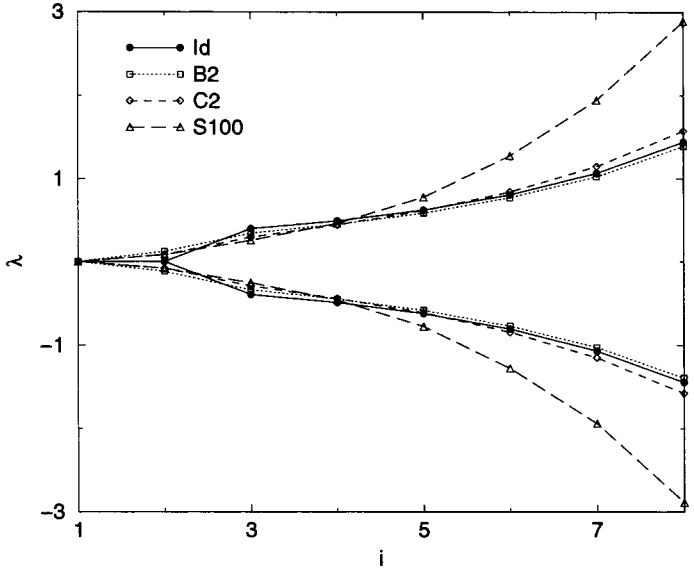

Fig. 1. Lyapunov spectra for a four particle system with density $\bar{n}=0.2$ in equilibrium. The solid line shows the spectrum for elastic reflection, i.e., the identity map is used instead of a chaotic one. The other spectra are obtained by using a baker map with $k=2$, a cat map with $k=2$ and a standard map with $k=100$, see Eqs. (24)–(26).

B. NSS

We move now on to the nonequilibrium stationary state and turn first to the case of an imposed temperature gradient by the walls. Since in the thermodynamic limit the Lyapunov spectrum is mainly determined by the bulk behavior we use in the following only a cat map with $k = 2$ as chaotic map $\mathscr{M}$. In order to determine the macroscopic state of the system the velocity and density profiles of the bulk are measured as well as the temperatures and velocities of the walls. Wall velocities are defined as the mean tangential velocity of the incoming and outgoing particles. Wall temperatures are defined as mean temperature of the incoming and outgoing fluxes, $\bar{T} = (\bar{T}_i + \bar{T}_o)/2$, with $\bar{T}_{i/o} = (\langle (v_x - \langle v_x \rangle_x)^2 \rangle_x + [v_y]_y / [v_y^{-1}]_y)/2$ where $\langle\ \rangle_x$ and $[\ ]_y$ represent an average over the density $\rho(v_x)$ and the flux Φ to and from the wall, respectively (see also ref. 17).

1. Heat Flow. Again, we first investigate a small system with four particles at $\bar{n} = 0.2$ with high accuracy. As already mentioned, in order to impose a temperature difference on the system we only have to choose two different parametrical temperatures T_u, T_d (see Eq. (2) and ref. 17). Note that this also affects the derivatives of the collision matrix (Eqs. (22) and (23)). Figure 2 shows the spectra for this system under a temperature

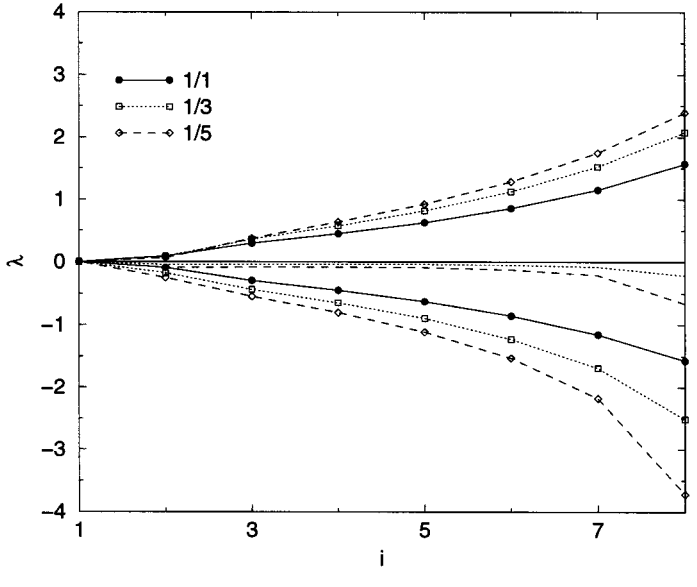

Fig. 2. Lyapunov spectra for a four particle system at density $\bar{n} = 0.2$ in NSS. The imposed temperatures for the upper and the lower wall are indicated by the numbers. The respective pair sums (scaled by a factor 1/2 for graphical reasons) are also plotted near the middle line.

gradient, the numbers denoting the parametrical temperatures $T_{u/d}$ of the upper and the low wall. In NSS the sum of the Lyapunov exponents is negative and exactly equal to the phase space contraction rate. The latter has been computed independently from the determinant of the scattering matrix (see also ref. 17) in order to check the algorithm. $T_u - T_d = 1 - 3$ results in $\sum \lambda_l = -1.029$ and $T_u - T_d = 1 - 5$ in $\sum \lambda_l = -2.703$. We find again two vanishing Lyapunov exponents but with increasing temperature difference all nonhero exponents also increase in magnitude, the negative ones certainly stronger to yield an overall negative sum. The pair sums are also shown and, as we expect, the driving shifts the sums towards negative values thus destroying the symmetry. The deviations from the pairing rule are particularly strong for pairs with large *i*. Figure 3 shows the results for a 36-particle system under the same setting. At least $2 \cdot 10^6$ disk-disk collisions and $2 \cdot 10^5$ disk-wall collisions have been simulated in each run. The spectra are plotted as connected line only for graphical reasons, it is understood that the exponents are defined for integer i only. The change in the Lyapunov spectrum under thermal driving are similar to the four-particle system. Increasing the density from $\bar{n} = 0.2$ to $\bar{n} = 0.6$ results in a larger magnitude of all nonzero exponents due to the higher collision rate. The Kaplan–Yorke dimension D_{KY} (Fig. 4) is decreasing for increasing temperature gradient, with a larger dimensionality loss ΔD_{KY} for higher densities than for lower densities at given $\Delta \bar{T}$. As can immediately be guessed from the positive branch of the spectra thermal driving also results in an increasing Kolmogorov–Sinai entropy h_{KS} (Fig. 4), defined as the sum over all positive exponents.

$$h_{\mathrm{KS}} = \sum_{\{\lambda_l > 0\}} \lambda_l \tag{27}$$

with increasing temperature gradient. Higher collision rates at higher densities lead to more viscous heating in the bulk and eventually to an increasing disorder (h_{KS}) of the system. The second, lower data point at $\Delta T = 0$ shows h_{KS}/N for elastic reflection as reference.

2. Shear Flow. First, let us take model I (Eqs. (3) and (4)) to induce a shear flow. Certainly, the drift also affects the derivatives of the collision matrix, Eqs. (22) and (23), where p_x^f goes to $p_x^f - d$ and p_x^i to $p_x^i + d$. Figure 5 shows the full Lyapunov spectra and the pair sums for a 36-particle system at $\bar{n} = 0.6$ under shear while keeping $T_u = T_d = 1$ fixed. The negative exponents increase in magnitude whereas the positive branch changes very little. Before we take a closer look at the Kaplan–Yorke dimension and the Kolmogorov–Sinai entropy let us investigate model III

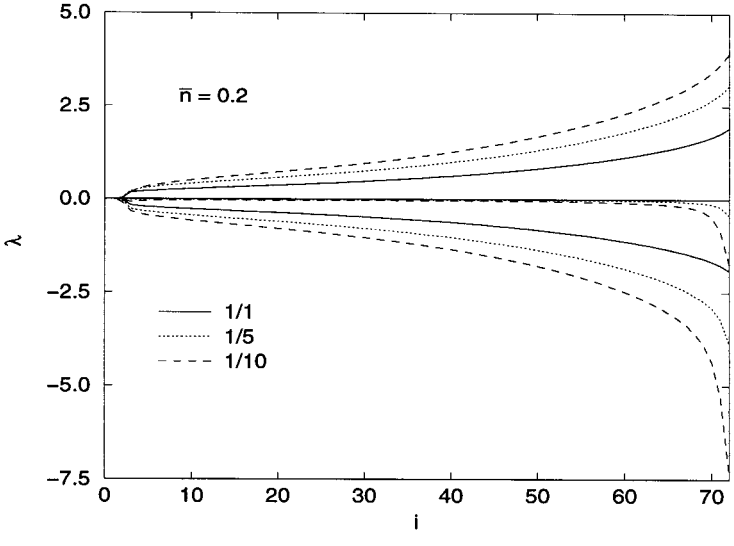

(a)

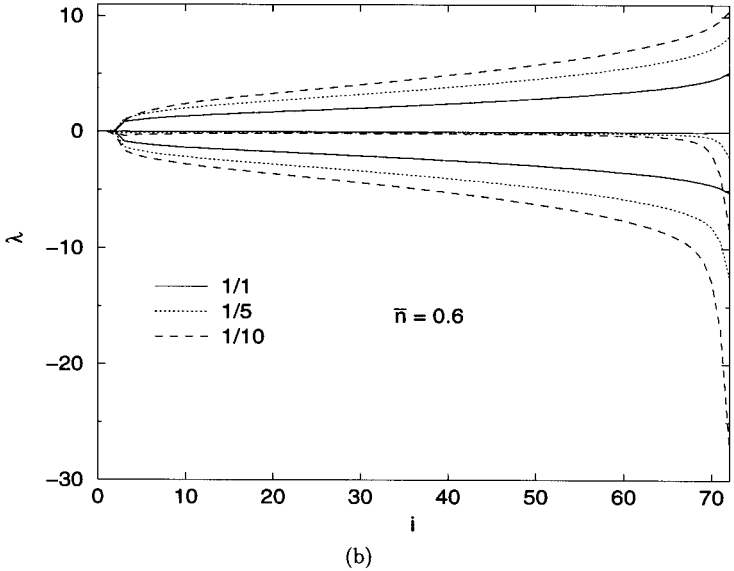

(b)

Fig. 3. Full Lyapunov spectra for a 36-particle system under an imposed temperature gradient at number densities $\bar{n} = 0.2$ and $\bar{n} = 0.6$. The numbers indicate the parametrical temperatures T_u, T_d. The respective pair sums (scaled by a factor 1/2 for graphical reasons) are also plotted near the middle line.

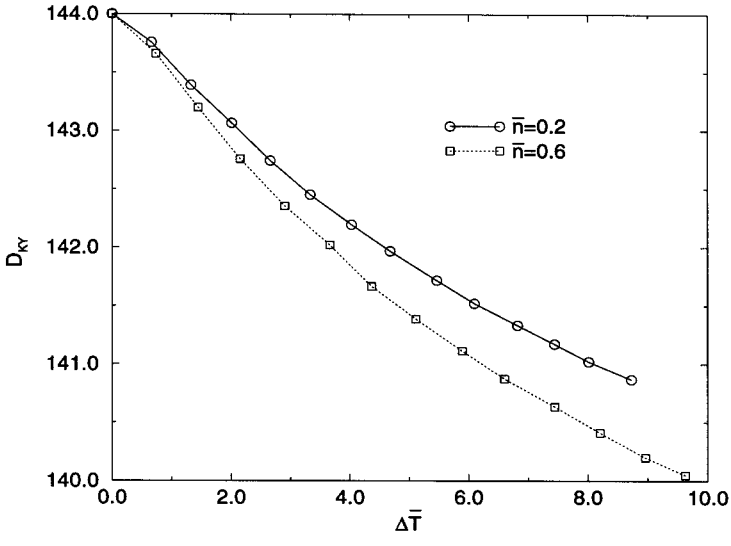

Fig. 4. The Kaplan–Yorke dimension D_{KY} and the Kolmogorov–Sinai entropy h_{KS} per particle for a 36-particle system under a temperature gradient at number densities $\bar{n}=0.2$ and $\bar{n}=0.6$. $\Delta\bar{T}$ denotes the measured temperature difference between the upper and the lower wall. The second, lower data point at $\Delta\bar{T}=0$ gives h_{KS}/N for elastic reflection as reference.

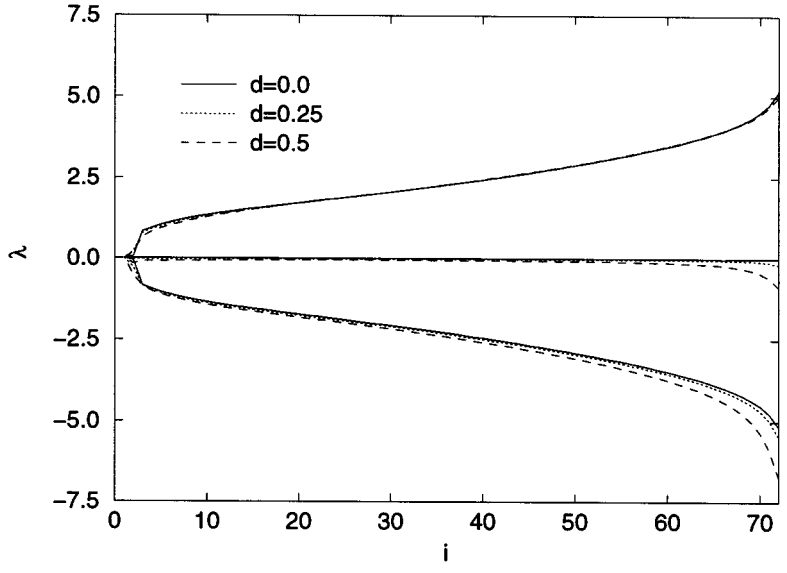

Fig. 5. Full Lyapunov spectra for a 36-particle system under shear at number density $\bar{n} = 0.6$, model I.

(Eqs. (5) and (6)). Note that p_x^f changes now to $p_x^f - d$ and p_x^i to $p_x^i - d$ in Eqs. (22) and (23). Figure 6 shows the corresponding Lyapunov spectra for a 36-particle system at $\bar{n} = 0.6$ under shear, but in contrast to model I the Lyapunov exponents of both the positive and the negative branch now increase in magnitude with increasing shear rate γ. For comparison the Lyapunov spectrum for the Chernov–Lebowitz model is also plotted, with E_{kin}/N and γ equal to values obtained with model III at $d = 1.5$. D_{KY} for both models is compared in Fig. 7(a) and we see that the dimensionality loss with increasing shear rate γ is stronger for model I than for model III. The graph of h_{KS}, plotted for both models in Fig. 7(b), asks for more explanation. Firstly, the overall behavior of h_{KS} is increasing with larger γ, which seems to be the opposite of the observation made for the Chernov–Lebowitz shear model in ref. 19. But there the total kinetic energy is keep constant for all shear rates whereas here both models try to fix the wall temperature. Increasing shear results in an increasing viscous heat production in the bulk which is reflected by a larger mean kinetic energy per particle (Fig. 8(a)). Hence, the loss in h_{KS} due to the ordering introduced by the shear is more than compensated by an increase of disorder due to a higher temperature in the bulk. Secondly, the only minor changes is the positive branch of the Lyapunov spectra for model I under shear yield an initially almost constant or even decreasing Kolmogorov–Sinai entropy.

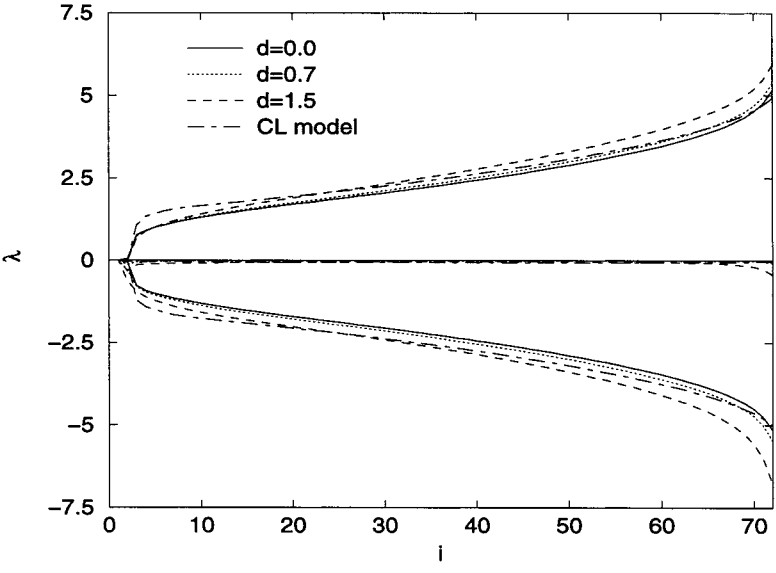

Fig. 6. Full Lyapunov spectra for a 36-particle system under shear at number density $\bar{n} = 0.6$, model III. The spectrum for the Chernov–Lebowitz model results from a simulation with the same mean kinetic energy per particle and approximately the same shear rate as model III with $T_u = T_d = 1.0$ and $d = 1.5$.

This, and the even more puzzling behavior of the wall temperature (Fig. 8(b)) can be explained by the fact that model I does *not* produce a Gaussian outgoing flux after the scattering. We found in ref. 17 that model I leads to an outgoing distribution with strong discontinuities in NSS whereas model III yields proper outgoing Gaussians. For comparison we have also computed D_{KY}, h_{KS} and the sum of the Lyapunov exponents for the Chernov–Lebowitz model when it is approximately in the same macroscopic state as models I and III, i.e., we set the Chernov–Lebowitz system on the same kinetic energy shell and tried to find the appropriate shear parameter which results in the same shear rate. The Kaplan–Yorke dimension seems to be almost identical with that of model III, Fig. 7(a), although the contraction rate, Fig. 9, is clearly different for larger shear rates. With regard to the previous work, this means that model III and the CL-model converge differently to an equality between phase space contraction and entropy production rates. Furthermore, the Kolmogorov–Sinai entropy now also increases with larger shear rate, only differing by a constant with the one obtained from model III, Fig. 7(b). This offset, depending on the special type of chaotic map chosen, originates from the fluctuating character of the model and should vanish in the thermodynamic limit.

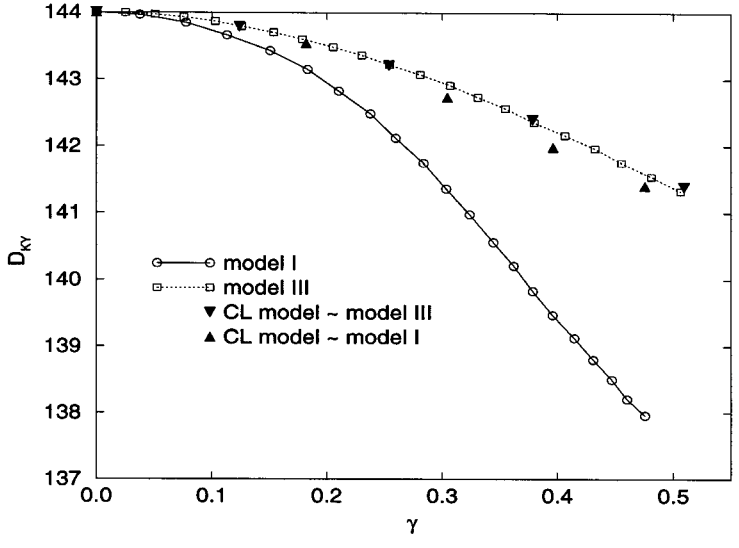

(a)

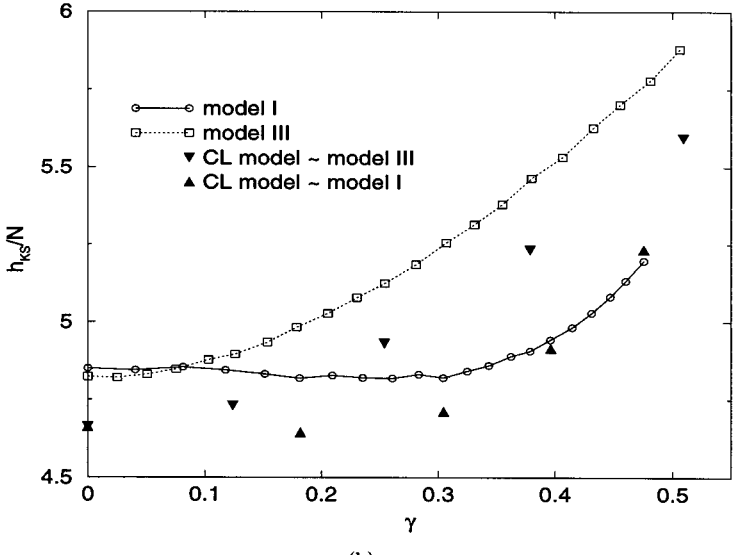

(b)

Fig. 7. The Kaplan–Yorke dimension D_{KY} and the Kolmogorov–Sinai entropy h_{KS} per particle for a 36-particle system under shear at number density $\bar{n} = 0.6$ as a function of the shear rate γ (model I, model III and Chernov–Lebowitz model).

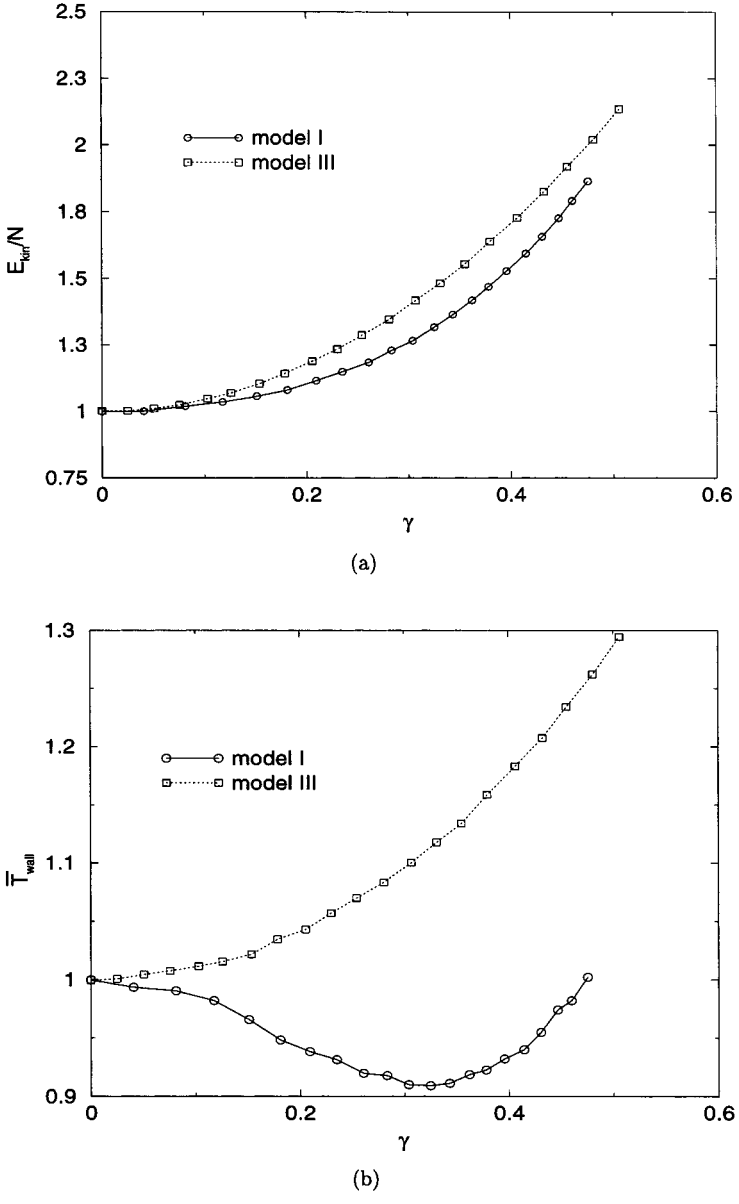

Fig. 8. Kinetic energy per particle and measured wall temperature for a 36-particle system under shear at number density $\bar{n} = 0.6$ as a function of the shear rate γ (model I and model III).

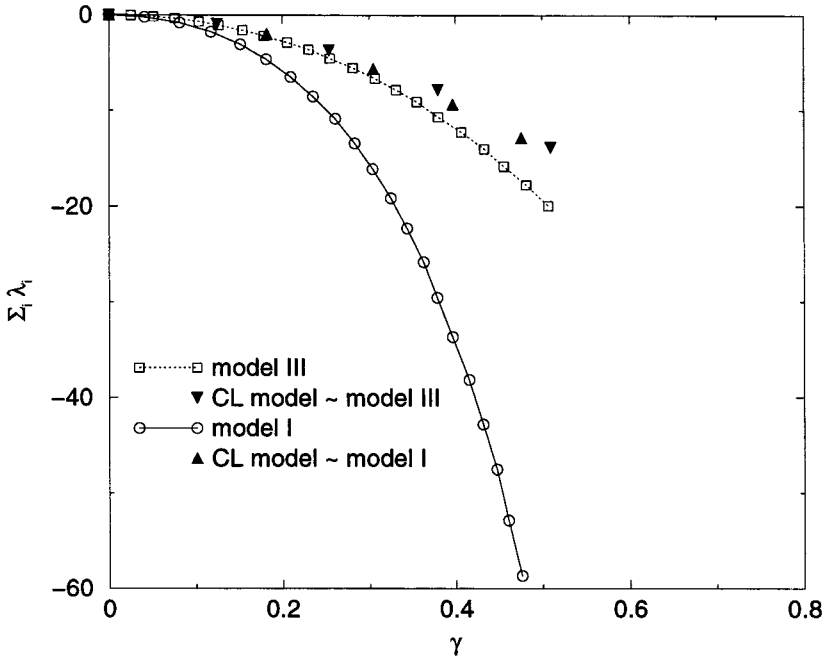

Fig. 9. Sum of Lyapunov exponents for a 36-particle system under shear at number density $\bar{n} = 0.6$ as a function of the shear rate γ (model I and model III and Chernov–Lebowitz model).

Finally, we remark that model I does not show any of these similarities with the CL-model, but is nevertheless a time reversible deterministic thermostat.

V. CONCLUSION

We have calculated the full Lyapunov spectrum for a hard-disk fluid in equilibrium and nonequilibrium steady state, thermostated by deterministic scattering. Since the model allows for fluctuations around a mean total energy only two vanishing Lyapunov exponents are found in both equilibrium and nonequilibrium states. In nonequilibrium the system is dissipative with a mean phase-space contraction rate smaller than zero. The magnitude of the Lyapunov exponents increase with increasing temperature gradient or shear rate, with a stronger increase for the negative branch. Thus both heat and shear flow situations result in a decreasing Kaplan–Yorke dimension and an increasing Kolmogorov–Sinai entropy with increasing nonequilibrium. Due to the inhomogeneous driving at the

boundary the pairing rule for Lyapunov exponents does not hold. This is also the reason why we did not verify a relation between Lyapunov exponents and transport coefficients (as, e.g., in ref. 21) since in absence of the pairing rule this should be tantamount to checking the relation between phase space contraction and entropy production rates, where the latter has already been done in ref. 17. The main difference of our shear flow model and the Chernov–Lebowitz shear flow model is the fact that in the latter the total kinetic energy is fixed whereas our models tries to fix the wall temperature. A direct comparison of shear flow model III and the CL-model reveals that they yield identical Kaplan–Yorke dimensions (within error bars) and only differ by a constant in the Kolmogorov–Sinai entropy, which vanishes in the thermodynamic limit.

ACKNOWLEDGMENTS

Special thanks go to C. Dellago for providing and explaining the original code used to compute the Lyapunov spectra and for helping to interpret the results. Furthermore, the author likes to thank O. Agullo for his technical support and R. Klages, F. Lekien, M. Louis and G. Nicolis for their helpful advice. This work is supported, in part, by the Interuniversity Attraction Pole program of the Belgian Federal Office of Scientific, Technical and Cultural Affairs and by the Training and Mobility Program of the European Commission.

REFERENCES

1. D. Evans, *J. Chem. Phys.* **78**:3297 (1983).
2. W. Hoover, A. Ladd, and B. Moran, *Phys. Rev. Lett.* **48**:1818 (1982).
3. D. Evans *et al.*, *Phys. Rev. A* **28**:1016 (1983).
4. S. Nosé, *Mol. Phys.* **52**:255 (1984).
5. S. Nosé, *J. Chem. Phys.* **81**:511 (1984).
6. W. Hoover, *Phys. Rev. A* **31**:1695 (1985).
7. M. Allen and D. Tildesley, *Computer Simulation of Liquids* (Clarendon Press, Oxford, 1987).
8. J. Lebowitz and H. Spohn, *J. Stat. Phys.* **19**:633 (1978).
9. A. Tenenbaum, G. Ciccotti, and R. Gallico, *Phys. Rev. A* **25**:2778 (1982).
10. S. Goldstein, C. Kipnis, and N. Ianiro, *J. Stat. Phys.* **41**:915 (1985).
11. N. Chernov and J. Lebowitz, *Phys. Rev. Lett.* **75**:2831 (1995).
12. N. Chernov and J. Lebowitz, *J. Stat. Phys.* **86**:953 (1997), 0022–4715.
13. W. Hoover and H. Posch, *Phys. Lett. A* **246**:247 (1998).
14. H. Posch and W. Hoover, *Phys. Rev. E* **58**:4344 (1998).
15. R. Klages, K. Rateitschak, and G. Nicolis, Thermostating by Deterministic Scattering, preprint, University of Brussels, chao-dyn/9812021 (1998).
16. K. Rateitschak, R. Klages, and G. Nicolis, Thermostating by Deterministic Scattering: The Lorentz gas, preprint, University of Brussels (1999).

17. C. Wagner, R. Klages, and G. Nicolis, *Phys. Rev. E* **60**:1401 (1999).
18. C. Dellago, H. A. Posch, and W. G. Hoover, *Phys. Rev. E* **53**:1485 (1996).
19. C. Dellago and H. A. Posch, *J. Stat. Phys.* **88**:825 (1997).
20. V. I. Oseledec, *Trans. Moscow Math. Soc.* **19**:197 (1968).
21. D. J. Evans, E. G. D. Cohen, and G. P. Morriss, *Phys. Rev. A* **42**:5990 (1990).
22. J. Kaplan and J. A. Yorke, in *Functional Differential Equations and Approximation of Fixed Points*, H. O. Peitgen and H. O. Walther, eds. (Springer-Verlag, Heidelberg, 1997).
23. G. Benettin, L. Galgani, A. Giorgilli, and J.-M. Streclyn, *Meccanica* **15**:9 (1980).